JOURNAL OF PLANKTON RESEARCH | VOLUME 34 | NUMBER 9 | PAGES 761–777 | 2012

Laser fluorescence analysis of phytoplankton across a frontal zone in the California Current ecosystem

ALEXANDER M. CHEKALYUK[1]*, MICHAEL R. LANDRY[2], RALF GOERICKE[2], ANDREW G. TAYLOR[2] AND MARK A. HAFEZ[1]
[1]LAMONT-DOHERTY EARTH OBSERVATORY OF COLUMBIA UNIVERSITY, 61 RT. 9W, PALISADES, NY 10964, USA AND [2]SCRIPPS INSTITUTION OF OCEANOGRAPHY, 9500 GILMAN DR., LA JOLLA, CA 92093, USA

*CORRESPONDING AUTHOR: chekaluk@ldeo.columbia.edu

Received November 4, 2011; accepted in principle March 19, 2012; accepted for publication April 7, 2012

Corresponding editor: Zoe Finkel

Spatial variability of chlorophyll, phycobiliproteins, chromophoric dissolved organic matter and variable fluorescence (F_v/F_m) was analyzed across a deep-water density front in the Southern California Current Ecosystem using an Advanced Laser Fluorometer (ALF) calibrated to assess chlorophyll concentration (C_{chl}), total autotrophic carbon (AC) and *Synechococcus* carbon biomass (SYN). Three distinct autotrophic assemblages were identified. Fluorescence was found to be three to four times higher in cooler mesotrophic waters north of the front than in warm oligotrophic waters to the south. Northern waters were distinguished by a shallow pigment maximum dominated by a blue-water type of *Synechococcus* and by the presence of green-water *Synechococcus* and cryptophytes; only blue-water *Synechococcus* were detected at lower concentration south of the front. The highest C_{chl} and AC values, accompanied by elevated F_v/F_m and chlorophyll fluorescence per unit of C_{chl}, and minimal *Synechococcus* abundance, were found directly at the front in a 20–40 m deep layer dominated by diatoms. The covariation of F_v/F_m with nitrate concentration in this layer, along with the structural changes in the phytoplankton community, suggest that it had been generated by *in situ* processes rather than advection. Strong structural responses to the local hydrography were also revealed by high-frequency underway ALF surface sampling, which detected an abrupt transition from low to high SYN on the northern side of a sharp salinity gradient at the front. *Synechococcus*-specific phycoerythrin fluorescence (F_{PE12}) and SYN were highly correlated in surface waters ($R^2 = 0.95$), while F_{PE12}:SYN gradually increased with depth. Strong relationships were found for chlorophyll fluorescence versus C_{chl} ($R^2 = 0.95$) and AC ($R^2 = 0.79$).

KEYWORDS: fronts; fluorescence; phytoplankton; *Synechococcus*; biomass; chlorophyll; phycoerythrin; photophysiology; variable fluorescence; A-Front

INTRODUCTION

Oceanic frontal zones are often characterized by enhanced biological activity and variability (e.g. Boucher *et al.*, 1987; Franks, 1992a; 1992b; Claustre *et al.*, 1994; Belkin *et al.*, 2009; Bost *et al.*, 2009). The biological properties of frontal waters can be strongly affected by the gradients in physical and chemical properties of water masses across the fronts (Corredor *et al.*,

doi:10.1093/plankt/fbs034, available online at www.plankt.oxfordjournals.org. Advance Access publication May 16, 2012

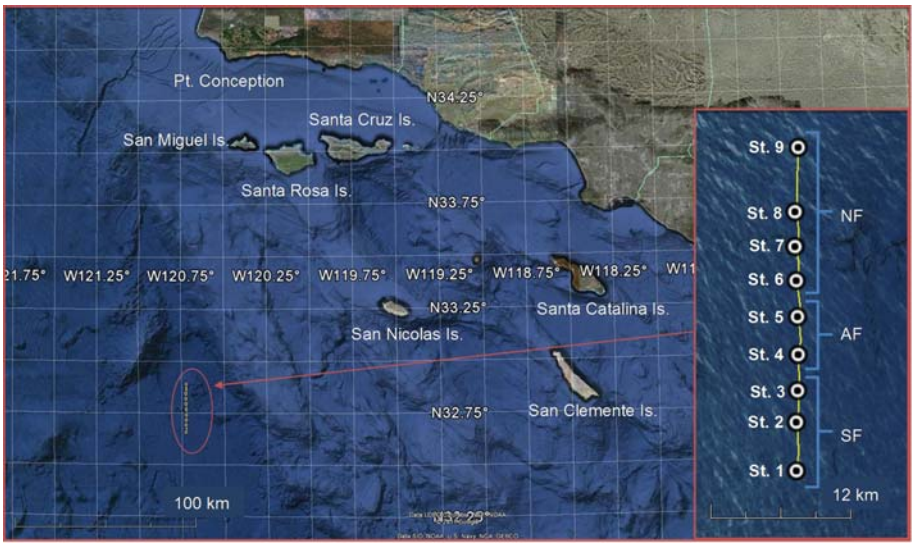

Fig. 1. Location of the A-front study and a map of the ALF underway transect measurements and cast stations. "SF", "AF" and "NF" mark the stations located to the south of the front, at the front and to the north of the front, respectively.

1987; Hitchcock *et al.*, 1994; Fernandez and Pingree, 1996; James *et al.*, 2002; Llido *et al.*, 2004; Baird *et al.*, 2008). Physical forcing may also impact the seasonal and interannual dynamics of phytoplankton in the shelf-slope frontal areas (Zhai *et al.*, 2011).

A variety of fluorescence-based approaches and sampling vehicles have been used to study phytoplankton distributions and responses to physical and chemical gradients in the oceans. Early studies demonstrated that *in vivo* measurements of chlorophyll fluorescence and physical parameters from towed platforms could be usefully combined with satellite observations for synoptic-scale analyses of biological and physical interactions (e.g. Trees *et al.*, 1992). Chlorophyll fluorescence measurements from various towed platforms and airborne laser fluorometry have been used as a proxy of phytoplankton biomass to study spatial distributions in relation to physical structures over small, meso and large scales (Hoge and Swift, 1981, 1983; Hitchcock *et al.*, 1994; Read *et al.*, 2002; Ashjian *et al.*, 2005). More recently, autonomous underwater vehicles and gliders, and in the present study, a Moving Vessel Profiler (Ohman *et al.*, 2012) have been successfully applied to quantify spatial variability in physical and bio-optical properties, including chlorophyll fluorescence, across frontal zones, eddies, thin layers and other physical structures (e.g. Yu *et al.*, 2002; Davis *et al.*, 2008; Frajka-Williams *et al.*, 2009; Hodges and Fratantoni, 2009; Johnston *et al.*, 2009).

Active saturation fluorometry has further allowed assessments of phytoplankton photosynthetic potential and physiological status in the ocean to study physiological responses to the physical–chemical gradients of frontal zones and eddies (e.g. Falkowski *et al.*, 1991; Falkowski and Kolber, 1995; Strutton *et al.*, 1997; Olson *et al.*, 2000; Moore *et al.*, 2003; Vaillancourt *et al.*, 2003; Holeton *et al.*, 2005). Similarly, fluorescence assessment of specific groups of phytoplankton by flow cytometry (FCM) and epifluorescence microscopy has opened the door to detailed analyses of composition, size, structure and rate responses of autotrophic communities across fronts and other physical features of the oceans (e.g. Hood *et al.*, 1992; Landry *et al.*, 2001, 2002, 2008; Jacquet *et al.*, 2002; Brown *et al.*, 2008).

Here, we present results of the laser fluorescence measurements in an offshore, seasonally persistent frontal zone formed by the convergence between the colder mesotrophic waters from the California Current and coastal upwelling area of California, and somewhat warmer oligotrophic waters (Niiler *et al.*, 1989; Haury *et al.*, 1993; Venrick 2000). The A-Front gradient was formed by eastward flow of the California Current and separated cooler mesotrophic waters of coastal upwelling origin to the north, from warm oligotrophic waters of mixed subarctic-subtropical origin to the south (Landry, Ohman *et al.*, 2012). The location of the area of study can be seen in Fig. 1. This study, conducted as part of the California Current Ecosystem Long Term Ecological Research (CCE-LTER) program, involved a new instrument, the Advanced Laser Fluorometer (ALF; see Table I for a list of acronyms, symbols and units) (Chekalyuk and Hafez,

Table I: List of abbreviations used in the text

Abbreviation	Term
AC	Total autotrophic carbon biomass, μg C L^{-1}
AC_{Diat}	Diatom carbon biomass, μg C L^{-1}
AC_F	Fluorescence estimate of total autotrophic carbon biomass, μg C L^{-1}
ALF	Advanced Laser Fluorometry/Fluorometer (method/instrument)
BV	Biovolume, a.u.
CDOM	Chromophoric dissolved organic matter (substance)
Chl *a*	Chlorophyll *a* (pigment)
C_{chl}	Chl *a* concentration, μg L^{-1}
C_{Fchl}	Fluorescence estimate of Chl *a* concentration, μg L^{-1}
F_{CDOM}	CDOM fluorescence, a.u.
F_{chl}	Chl *a* fluorescence, a.u.
F^g_{chl}	Chl *a* fluorescence measured with 532 nm excitation, a.u.
F^v_{chl}	Chl *a* fluorescence measured with 405 nm excitation, a.u.
FCM	Flow cytometry (method, technique)
F_{PC}	Phycocyanin fluorescence, a.u.
F_{PE1}	PE fluorescence of blue-water type of phototrophic cyanobacteria, a.u.
$F_{PE12} = F_{PE1} + F_{PE2}$	Total PE fluorescence of phototrophic cyanobacteria, a.u.
F_{PE2}	PE fluorescence of green-water type of phototrophic cyanobacteria, a.u.
F_{PE3}	PE fluorescence of eukaryotic cryptophytes, a.u.
F_v/F_m	Variable fluorescence of Chl *a in vivo*, dimensionless
HPLC	High-pressure liquid chromatography (method, technique)
Lat	Latitude, degrees
N	Number of regression points involved in the correlation analysis
PBP	Phycobiliprotein (pigments)
PE	Phycoerythrin (pigment)
SDC	Spectral deconvolution (method, technique)
SEE	Standard error of estimate (calculated from the correlation analysis)
SSS	Sea surface salinity, dimensionless
SST	Sea surface temperature, °C
Syn	*Synechococcus* spp. (phototrophic cyanobacteria)
SYN	*Syn*-specific carbon biomass, μg C L^{-1}
SYN_F	Fluorescence estimate of *Syn*-specific carbon biomass, μg C L^{-1}

2008). We used ALF to characterize cross-frontal distributions of chlorophyll *a* (Chl *a*), phycobiliprotein (PBP) pigments, chromophoric dissolved organic matter (CDOM) and variable fluorescence at sea in real time. Based on strong relationships between ALF fluorescence and contemporaneous measurements of the autotrophic community biomass and composition from high-pressure liquid chromatography (HPLC), FCM and digital epifluorescence microscopy, we documented substantial cross-frontal changes in phytoplankton characteristics, including a narrow zone of enhanced population response of *Synechococcus* in the area of sharp physical gradients at the front.

METHOD

Sampling plan

The A-Front study was conducted during the nighttime (dark) hours of 24–25 October 2008 during a research cruise of the R/V *Melville* southwest of San Nicolas Island off southern California (Fig. 1). A 25-km transect line located orthogonally to the east–west oriented frontal feature was covered (Landry, Ohman *et al.*, 2012). Beginning about one-half hour after sunset (extending from 18:34 to 20:56 local time), the transect was occupied from north to south in continuous underway survey mode to yield highly resolved fluorescence measurements of surface features. Then it was immediately resampled south-to-north with CTD-rosette casts at nine stations for fluorescence measurements and plankton community samples at 7–8 discrete depths to 100 m. Preceding transect sampling, we used satellite imagery (Kahru *et al.*, 2012) and real-time underway measurements with ALF and a Moving Vessel Profiler system (Ohman *et al.*, 2012) to identify the front and to select the locations of the sampling stations. Underway measurements were made on a total of five crossings of the front at different locations, but only the final run, taken in darkness, is used here to describe fine-scale surface structure of the front. In the transect line depicted in Fig. 1, sampling Stations 1, 2 and 3 are located to the south of the front (32.667 to 32.725°N), Stations 4 and 5 are located directly in the frontal zone (32.750 and 32.775°N) and Stations 6–9 are north of the front (32.803 to 32.896°N). These station groups are, respectively, marked as SF, AF and NF.

ALF measurements

Two custom-built ALF instruments were used for the measurements of underway fluorescence and for discrete sample analysis during the A-Front station sampling. The ALF is a portable benchtop instrument that combines high-resolution spectrally and temporally resolved flow-through measurements of the laser-stimulated emission from seawater (Chekalyuk and Hafez, 2008). Two excitation wavelengths, 405 and 532 nm, are used for the measurements. Real-time spectral deconvolution (SDC) provides assessment of several aquatic fluorescence constituents, including Chl *a*, PBP pigments and CDOM. The intensities of the constituent-specific fluorescence bands are normalized to the intensity of the water Raman scattering to improve the accuracy of fluorescence assessments (Klyshko and Fadeev, 1978; Hoge and Swift, 1981). The Raman-normalized, instrument-independent fluorescence parameters can be directly compared with data

measured by other laser spectrofluorometers, including shipboard and airborne LIDAR fluorosensors (e.g. Cowles *et al.*, 1993; Chekalyuk *et al.*, 1995; Wright *et al.*, 2001).

The SDC algorithm provides detection and quantification of three spectral types of phycoerythrin (PE) fluorescence used for characterization of blue- and green-water types of phototrophic cyanobacteria *Synechococcus* spp. (*Syn*) and eukaryotic cryptophytes (F_{PE1}, F_{PE2} and F_{PE3} with spectral maxima at 565, 578 and 590 nm, respectively; all water Raman-normalized). In the following sections, F_{chl}, F_{CDOM}, $F_{PE12} = F_{PE1} + F_{PE2}$ and F_{PC} denote Raman-normalized intensities of Chl *a*, CDOM, *Syn*-specific PE and phycocyanin fluorescence bands, respectively. Superscripts "v" and "g" are used below to denote Chl *a* fluorescence retrieved from seawater emission spectra measured using the violet and green excitation wavelengths that differ in the excitation efficiency and result in different fluorescence intensities, F^{v}_{chl} and F^{g}_{chl}. In addition, we used temporally resolved and spectrally corrected for non-Chl *a* background emission (Chekalyuk and Hafez, 2008) measurements of Chl *a* variable fluorescence, F_v/F_m, to assess the photochemical efficiency and photophysiological status of the autotrophic community. Detailed information about the ALF instrument, measurement protocols and analytical algorithms is given by Chekalyuk and Hafez (Chekalyuk and Hafez, 2008).

During the underway measurements, ALF was connected to the shipboard uncontaminated seawater system that continuously pumped surface water from 4.5 m at the bow of the ship. A total of 1560 measurements were automatically made after sunset (18:09), between 18:35 and 20:56 October 24 2008 along the 25-km transect line across the front. For discrete sample analyses, fluorescence measurements were averaged over a 400 mL sample volume that passed by the detectors at a flow rate of 100 mL min^{-1}. The seawater samples were collected at night with Niskin bottles at various depths and kept in the dark in amber glass bottles for ~40 min before the measurements to preserve a dark-adapted state of phytoplankton (Chekalyuk and Hafez, 2008). The ALF measurements of the dark-adapted phytoplankton are compliant with the "four-step measurement protocol" that allows the photophysiological variability in Chl *a* fluorescence (Kiefer, 1973; Stramska and Dickey, 1992; Bricaud *et al*, 1995; Marra, 1997) to be minimized, thus improving the accuracy of fluorescence assessments of pigment biomass (Chekalyuk and Hafez, 2011). Since both discrete sample analysis and underway fluorescence measurements were conducted in the dark-adapted state of phytoplankton, the relationships between the ALF fluorescence measurements and independent retrievals of Chl *a* concentration and phytoplankton biomass derived from the discrete sample analysis could be used to assess these two important characteristics from the high-resolution underway fluorescence measurements (see below). If the underway fluorescence measurements were conducted during daytime and affected by the solar-induced non-photochemical quenching [NPQ, e.g. (Krause and Weis, 1991)], the concurrent measurements of variable fluorescence could be used to adjust the Chl *a* fluorescence retrievals for the NPQ effect and ensure the accurate fluorescence assessments of pigment biomass (Chekalyuk and Hafez, 2011).

Chlorophyll concentration and phytoplankton biomass

During station sampling with the CTD rosette, water samples were taken from the same Niskin bottles as the samples used for the ALF measurements, in order to compare and calibrate the fluorescence readings against independent estimates of chlorophyll *a* concentration and phytoplankton carbon biomass. Chl *a* concentration (μg L^{-1}) was determined from HPLC analyses of 2.2- or 4.4-L samples, which were filtered onto Whatman GF/F filters, stored in liquid nitrogen and extracted in acetone as described by Goericke (Goericke, 2002). The pigment was analyzed on an Agilent 1100 series HPLC system (Agilent Technologies, Santa Clara, CA, USA) with a Waters Symmetry C8 column (3.5-μm particle size, 4.6 × 150 mm, silica, reverse-phase; Waters, Milford, MA, USA), using canthaxanthin as an internal standard.

Photosynthetic bacteria were enumerated by FCM in 2 mL samples preserved with 0.5% paraformaldehyde (final concentration) and frozen in liquid nitrogen. The samples were thawed in batches, stained with Hoechst 34442 (1 μg/mL, final concentration) and analyzed on a Beckman–Coulter Altra flow cytometer equipped with a Harvard Apparatus syringe pump and two argon ion lasers tuned to UV (200 mW) and 488 nm (1 W) (Selph *et al.*, 2011). Listmode data files of cell fluorescence and light-scatter properties were normalized to internal standards of fluorescent beads and processed using the FlowJo software (Tree Star, Inc., www.flowjo.com) to define population abundances of *Prochlorococcus* and *Synechococcus* spp. These cell abundances were converted to biomass using mixed-layer estimates of 32 and 101 fg C $cell^{-1}$, respectively (Garrison *et al.*, 2000).

Biomass assessments (μg C L^{-1}) of eukaryotic phytoplankton were made by digital epifluorescence microscopy (Taylor *et al.*, 2012). Seawater samples (500 mL)

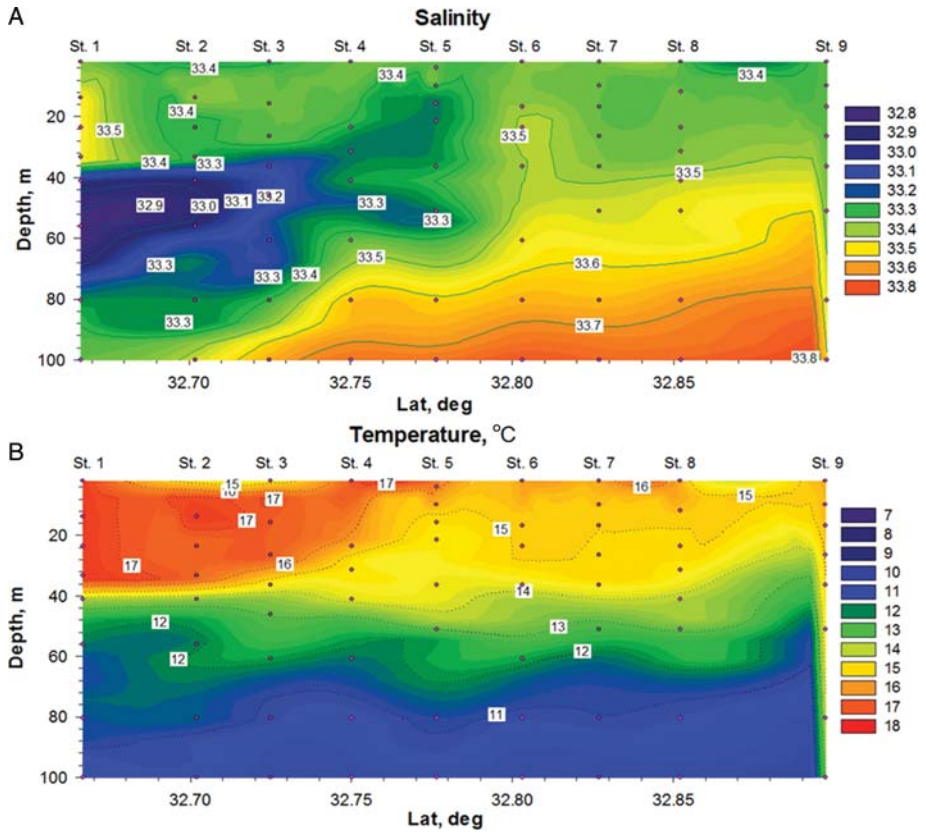

Fig. 2. Distributions of seawater salinity (**A**) and temperature (**B**) in the euphotic layer across the A-front. The locations of water sampling with the CTD casts here and in the following plots are marked with the dark-red dots.

were preserved and cleared according to a modified protocol from Sherr and Sherr (Sherr and Sherr, 1993), with sequential additions of 260 μL of alkaline Lugol's solution, 10 mL of buffered formalin and 500 μL of sodium thiosulfate, and then stained with 1 mL of proflavin (0.33% w/v) and 1 mL of DAPI (0.01 mg mL^{-1}). Aliquots of 50 mL were filtered onto a 25 mm, 0.8 μm pore black polycarbonate filters to determine concentrations of nanophytoplankton and the remaining 450 mL samples were filtered onto black 8.0 μm polycarbonate membranes to determine concentrations of larger cells (microplankton). Each filter was mounted onto glass slides using immersion oil and a No. 2 cover slip. All slides were digitally imaged using a Zeiss Axiovert 200 M inverted compound microscope. Digital images were acquired at >20 positions per slide with a Zeiss AxioCam HRc color CCD digital camera at ×630 (nanoplankton) and ×200 (microplankton).

The resulting images were processed and analyzed using the ImagePro software. Eukaryotic phytoplankton were distinguished from heterotrophic protists or nonliving particles by the presence of a defined nucleus (DAPI blue fluorescence) and strong Chl *a* (red) fluorescence. Biovolumes (BVs; μm^3) were calculated from the length (L) and width (W) measurements of each cell using the geometric formula of a prolate sphere ($BV = 0.524LWH$), where unmeasured height (H) was estimated as W for diatoms and $0.5W$ for flagellates (Taylor *et al.*, 2011). Biomass was calculated as carbon (C; pg $cell^{-1}$) using the equations of Menden-Deuer and Lessard (Menden-Deuer and Lessard, 2000): $C = 0.288 \times BV^{0.811}$ for diatoms and $C = 0.216 \times BV^{0.939}$ for non-diatoms.

RESULTS

Distributions of physical characteristics and nutrients across the frontal zone

The physical and chemical settings of the study area are discussed in detail in companion articles (Landry, Ohman *et al.*, 2012; Li *et al.*, 2012). Here, we briefly summarize the main features of the temperature and salinity distributions in the euphotic layer (Fig. 2) that are referred to below when discussing the fluorescence patterns. The A-Front was sharply delineated by a 16°C

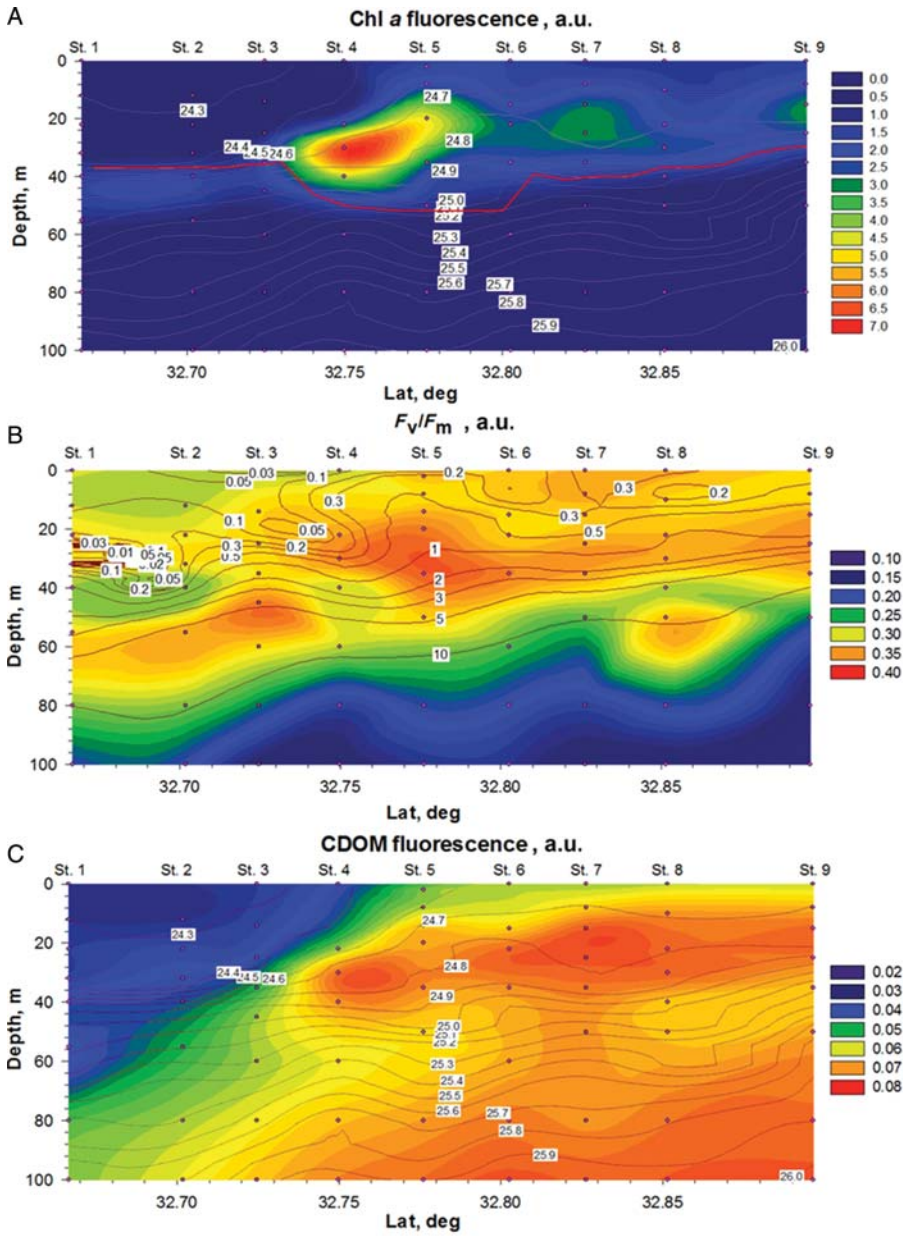

Fig. 3. Spatial distributions of Chl *a* fluorescence (**A**), variable fluorescence (**B**) and CDOM fluorescence (**C**) in the euphotic layer across the frontal zone. (A) The pycnocline is marked with a red line; gray solid lines display isopycnals. (B) Dark solid lines display iso-nitrate distribution; nitrate concentrations, μM, are displayed with numbers. (C) Solid contour lines display isopycnals. The frontal feature was located between Stations 4 and 5 (Figs 2 and 8).

isotherm at the surface and by a 33.4 isohaline at depths of 10–90 m. Salinity varied in the range of 33.4–34.5 over most of the mixed layer to the south and north of the front (centered on Stations 4 and 5, Fig. 2A). Below the mixed layer, cold and fresh waters characteristic of the California Current were found south of the front at depths of 40–80 m. The spatial distribution of salinity suggests diapycnal mixing of this water mass at the front (Li *et al.*, 2012). Such mixing resulted in somewhat lower salinity values in the upper portion of the euphotic layer (10–40 m) at the front (Fig. 2A).

Spatial patterns of temperature (Fig. 2B) and nutrients (see iso-nitrate contour lines in Fig. 3B) are consistent with this interpretation. In particular, the mixing of colder and warmer waters is evident in temperature values in the upper 40 m at the front (Stations 4 and 5). Nitrate concentration (0.4 μM) was also elevated in the

surface layer at the front relative to the areas to the north and south (Fig. 3B). The lowest nutrient concentrations were found in the distinct warm ($T > 16^{\circ}C$) water of the upper 40 m mixed layer located south of the front (Stations 1–3), which was separated by a sharp pycnocline from the colder and fresher waters of the California Current. Nutrient concentrations in the colder mixed layer north of the front (Stations 6–9) were somewhat lower than at the front, but several times greater than the mixed-layer concentrations south of the front (Stations 1–3).

Fluorescence patterns

A subsurface F_{chl} maximum of variable intensity and depth was detected across the frontal zone and adjacent areas (Fig. 3A). The most intense F_{chl} patch was found at ~35 m depth directly at the front (Station 4). In this area, F_{chl} was ~2-fold higher than in the shallow maximum north of the front (~15 m, Station 7), and three to four times higher than in the deeper maximum (45 m, Stations 1–3) south of the front. The maximum fluorescence layers were located between the 24.7 and 24.8 isopycnals, slightly below the pycnocline at the southern stations and above the pycnocline at the front and northern stations.

The spatial patterns of variable fluorescence, a proxy of phytoplankton photophysiological status, (Fig. 3B) were generally more uniform than those of pigment fluorescence. The highest values of F_v/F_m (~ 0.4) were observed directly at the front (Station 5), just below the F_{chl} maximum at ~ 35 m, in the area of diapycnal frontal mixing [Fig. 2; for details see (Li *et al.*, 2012)] that resulted in the elevated nitrate concentrations (Fig. 3B). Another area of elevated F_v/F_m (up to 0.4) was detected between 40 and 60 m depth south of the front (Stations 1–3), in the tongue of cold, fresh California Current water (Fig. 2A). The F_v/F_m minimum of ~0.25 was coincident with the subsurface Chl *a* maximum at 40 m south of the front (Stations 1 and 2; Fig. 3A). A broad area of low F_v/F_m was also found at Stations 1–3 down to 18 m depth, indicative of the relatively depressed physiological status of phytoplankton in the low-nutrient southern surface waters. In contrast, the vertical distribution of F_v/F_m was more uniform in the upper 40 m of the euphotic layer, above the nitracline in the waters north of the front. The spatial pattern of F_v/F_m generally followed the nitrate distribution (Fig. 3B), with the highest values of F_v/F_m occurring below the depth of 3 μM nitrate south of the front and at or above the depth of 2 μM nitrate in the front and northern stations.

The distribution of CDOM fluorescence in the upper, mixed portion of the euphotic layer (Fig. 3C) generally followed the patterns of pigment fluorescence, suggesting a recent biological origin of CDOM. F_{CDOM} showed a sharp frontal gradient dividing the low F_{CDOM} water south of the front from the high F_{CDOM} waters to the north. The layer of elevated F_{CDOM} was also located between the 24.7 and 24.8 isopycnals, following F_{chl} distribution (Fig. 3A). The highest F_{CDOM} values were detected at 35 m on the front (Stations 4 and 5), near the F_{chl} peak (Fig. 3A). An almost equally intense F_{CDOM} maximum was detected throughout the northern area at ~25 m; it also coincided with the subsurface maxima of pigment fluorescence (Figs 3A and 4). A large area of low F_{CDOM} values (delineated by the 24.5 isopycnal in Fig. 3C) was found in the warm low-Chl surface water at the front, extending and deepening to the south. Below the mixed layer, CDOM fluorescence gradually increased with depth.

A strong core of F_{PE1} fluorescence indicative of blue-water *Syn* was detected at 25 m in the northern waters (Fig. 4A). The highest values of F_{PE1} were observed at Station 8, while low F_{PE1} values coincided with the F_{chl} maximum at the front (Stations 4 and 5). In the southern area, somewhat elevated F_{PE1} values were detected in the F_{chl} maximum at 40 m. However, F_{PE1} there was an order of magnitude lower than the subsurface maximum values at the northern stations.

A subsurface maximum of F_{PE2} fluorescence from green-water *Syn* was also found north of the front, with two areas of higher concentration at Stations 7 and 9 (30 and 25 m, respectively; Fig. 4B), straddling the stronger F_{PE1} subsurface maximum at Station 8 (Fig. 4A). Relatively low F_{PE2} fluorescence was found at the front (Stations 4 and 5), and no detectable F_{PE2} signal was measured on the southern side of the front. The F_{PE3} fluorescence of eukaryotic cryptophytes followed both spatially and quantitatively the pattern of F_{PE2}, except for a more substantial (50%) decline in the area of the major F_{PE1} maximum (Fig. 4C). As for F_{PE2}, no F_{PE3} fluorescence was detected in the southern area.

The fluorescence of phycocyanin, an accessory pigment present in both *Syn* and cryptophytes, integrated the major features of the F_{PE1}, F_{PE2} and F_{PE3} distributions (Fig. 4D). The F_{PC} peak coincided with the F_{PE1} maximum of blue-water *Syn* at Station 8. However, the area of high F_{PC} magnitude extended further south and north than the F_{PE1} maximum, reflecting the F_{PC} contributions of green-water *Synechococcus* spp. and cryptophytes. In contrast to the F_{chl} distribution (Fig. 3A), the PBP fluorescence maxima were located slightly deeper, just above the pycnocline in the northern area.

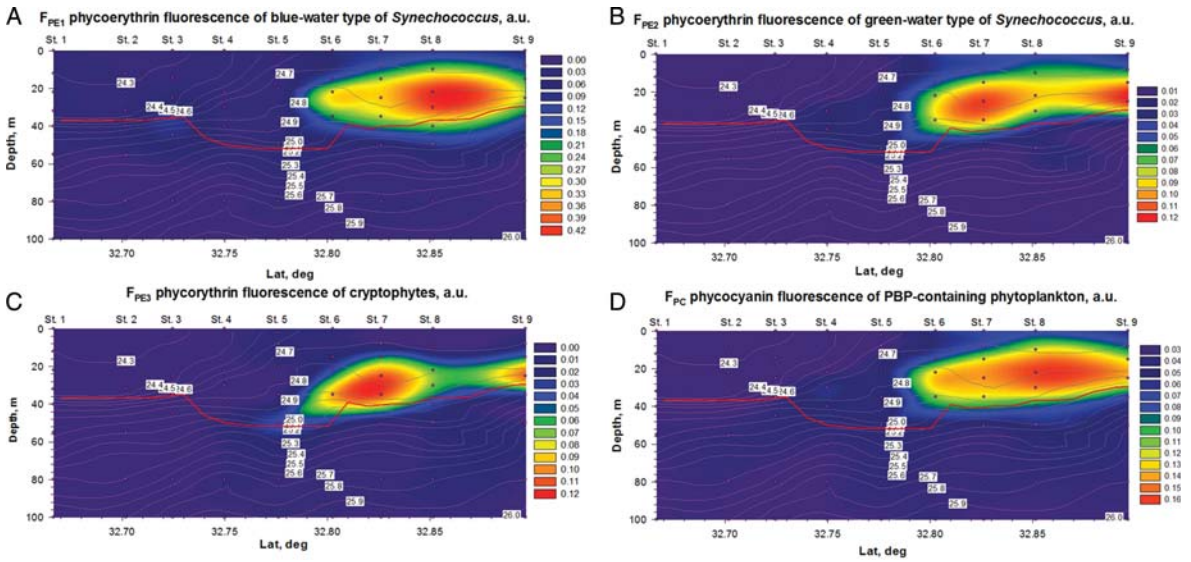

Fig. 4. Spatial distributions of PE fluorescence of blue-water (**A**) and green-water (**B**) types of *Synechococcus* and cryptophytes (**C**) in the euphotic layer across the frontal zone. (**D**) Distribution of phycocyanin fluorescence. The pycnocline is marked with a red line; gray solid lines display isopycnals. The frontal feature was located between stations 4 and 5 (Figs 2 and 8).

Correlation analyses

In vivo Chl *a* fluorescence is commonly used as a proxy for Chl *a* concentration or phytoplankton biomass. Similarly, the group-specific PE fluorescence measurements may provide proxies for the biomass of PBP-containing groups of phytoplankters, such as photosynthetic cyanobacteria or eukaryotic cryptophytes (Chekalyuk and Hafez, 2008). The A-Front study has provided a unique opportunity to explore the relationships between these variables in an area of strong gradients in physical and chemical properties of water masses over a relatively small spatial scale.

Spatial distributions of Chl *a* fluorescence (F_{chl}) (Fig. 3A) and Chl *a* concentration (C_{chl}) from HPLC pigment analyses (Fig. 3 in Taylor *et al.*, 2012) were found to be very similar across the frontal zone. The regression analysis revealed a high correlation between F_{chl} and C_{chl} [$R^2 = 0.95$ for F^g_{chl} (Fig. 5A), and $R^2 = 0.92$ for F^v_{chl} (not shown); a third-order polynomial regression was used]. The non-linear relationship between F_{chl} and C_{chl} suggests a gradual increase in F_{chl}:C_{chl} ratio with increasing $C_{chl.}$. On closer examination, one group of samples departed notably from others in the C_{chl} versus F_{chl} relationship (Fig. 5B). These were seven samples collected from the mixed layer at or above the strong subsurface Chl *a* maximum at the front, where large diatoms dominated autotrophic biomass (Taylor *et al.*, 2012). The locations of these samples are marked with cyan-colored dots in Fig. 6A, which displays the spatial distribution of diatom carbon biomass normalized to total autotrophic carbon biomass, AC_{Diat}/AC (determined from digital microscopic and flow cytometric analyses by Taylor *et al.*, 2012). For this diatom-dominated sampling area, Chl *a* fluorescence per unit Chl *a* was ~50% brighter than for other samples from the euphotic layer across the frontal zone. Both groups of samples showed high correlations ($R^2 = 0.92$ and 0.98, respectively), but still non-linear relationships between F_{chl} and C_{chl}.

The spatial distribution of Chl *a* fluorescence in Fig. 3A is also very similar to the pattern for autotrophic carbon (AC) calculated using microscopic and FCM analyses of the cast samples (Fig. 3 in Taylor *et al.*, 2012). For all water samples collected across the A-Front, Chl *a* fluorescence showed a strong linear relationship and high correlation with AC [$R^2 = 0.79$ for F^v_{chl} (Fig. 5C), and $R^2 = 0.72$ for F^g_{chl} (not shown)]. The subsets of data for the front stations, the northern area and samples from the upper 35 m of the southern area indicated no regional specifics and very similar correlation coefficients [e.g. $R^2 = 0.78$ ($N = 13$; SEE = 14.6), 0.79 ($N = 27$; SEE = 6.6), and 0.80 ($N = 11$; SEE = 1.7), respectively] for F^v_{chl} versus AC regressions, despite structural diversity of phytoplankton communities in these areas (Taylor *et al.*, 2012). However, samples collected below 40 m in the southern area (marked with open circles in Fig. 5C) showed a distinctly different linear regression relationship with high correlation coefficient ($R^2 = 0.97$), but an almost two-fold smaller slope (29 versus 53, see Fig. 5C). This suggests more intense Chl *a* fluorescence per unit of carbon biomass for the samples from this area, which was dominated by the

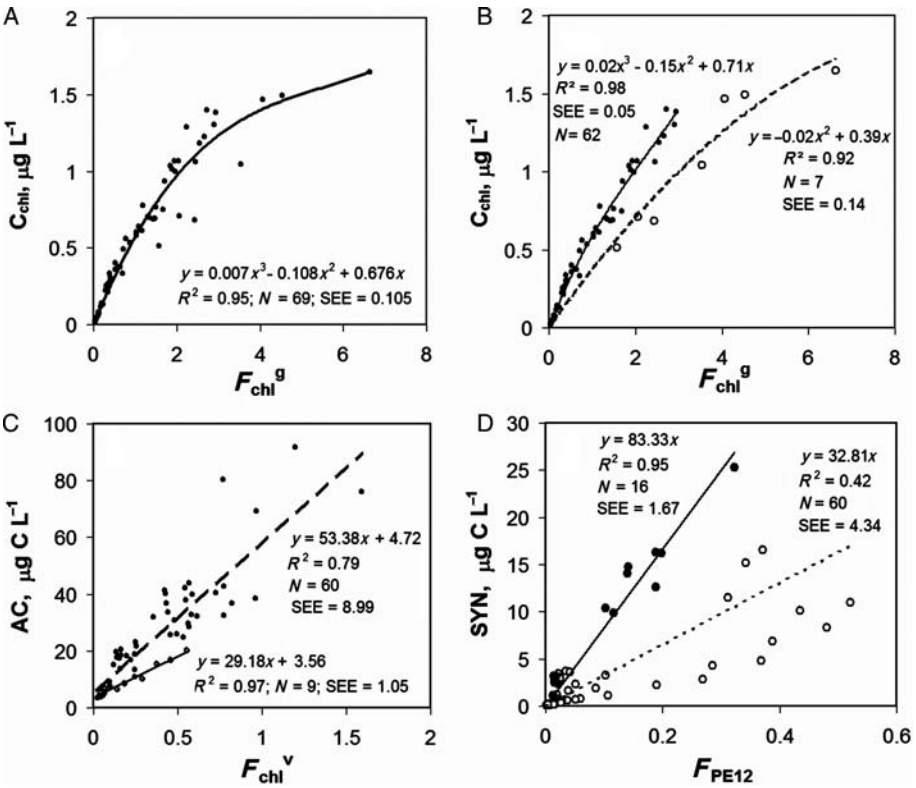

Fig. 5. (**A**) Correlation between Chl *a* concentration (C_{chl}) and Chl *a* fluorescence measured with green laser excitation (F^g_{chl}) in nighttime water samples. The sampling points are displayed with dark red dots in Figs 2–4. (**B**) Same data as in (A); a subset of samples from the diatom-dominated Chl *a* maximum at the front is displayed with empty circles. (**C**) Dashed line displays a linear regression between total autotrophic carbon biomass (AC) and Chl *a* fluorescence measured with blue laser excitation (F^v_{chl}) for the same set of samples as in (A); solid line displays the regression for a subset of samples collected between 40 and 80 m at stations 1–3. (**D**) Dashed line displays the regression between the *Syn*-specific PE fluorescence (F_{PE12}) and their carbon biomass (SYN); solid line represents the regression for a subset of the samples (filled circles) collected in the subsurface layer above the Chl *a* maximum (Fig. 3A). Here, R^2 is a correlation coefficient, N a number of data points and SEE a standard error of estimates.

autotrophic nanoplankton (2–20 µm cells) comprising up to 80% of total AC (Taylor *et al.*, 2012).

The regression equations $y = 0.007x^3 - 0.108x^2 + 0.676x$ (Fig. 5A) and $y = 53.38x + 4.72$ (Fig. 5C) were chosen for fluorescence assessments of Chl *a* concentration (C_{Fchl}) and total autotrophic carbon biomass (AC_F) using ALF measurements of F^g_{chl} and F^v_{chl}, respectively. Below, we use this approach to build the C_{Fchl} and AC_F spatial distributions in the euphotic layer (Fig. 6B and C) and to calculate high-resolution surface distributions of AC_F and C_{Fchl} from the ALF underway measurements of Chl *a* fluorescence. In this study, we found only minor difference between F^g_{chl} and F^v_{chl} in the degree of their correlation with both C_{chl} and AC (see above), which is consistent with results of our earlier field measurements. Thus, either F^g_{chl} or F^v_{chl} could have been used for the assessment of both C_{Fchl} and AC_F. Our choice of F^g_{chl} and F^v_{chl} fluorescence parameters for assessments of C_{Fchl} and AC_F, respectively, was based only on the slightly higher correlation coefficients calculated for F^g_{chl} versus C_{chl}, and F^v_{chl} versus AC, respectively.

While the vertical profiles of the *Syn*-specific PE fluorescence, F_{PE12}, and SYN biomass from FCM analyses showed generally similar patterns across the transect, the F_{PE12} maxima were consistently deeper than the SYN maxima in the study area (e.g. Fig. 7). For all nine stations, F_{PE12}:SYN ratios changed relatively little above the subsurface Chl *a* maxima, but they showed considerable, up to 10-fold, increase with depth in and below the Chl *a* maxima (Fig. 7). This can be explained by photo-acclimative increase in the PE cellular quotas under low-light conditions in deeper water layers, consistent with earlier observations (e.g. Vernet *et al.*, 1990; Bricaud *et al.*, 1995). It may also be attributable to larger size of *Syn* cells at depth (e.g. Binder *et al.*, 1996), which are not accounted for in the FCM cell carbon conversions (see Discussion). Other PBP fluorescence

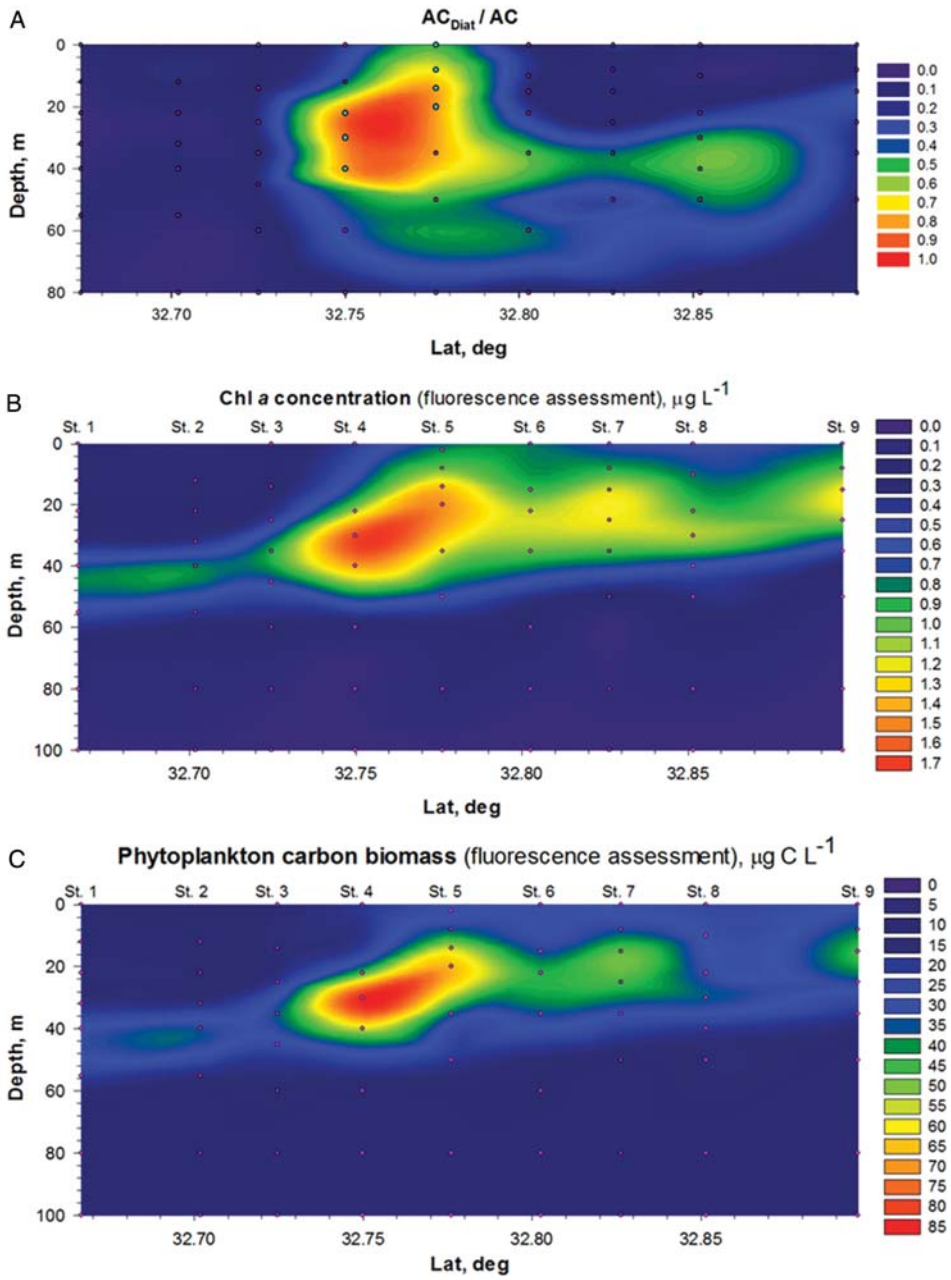

Fig. 6. (**A**) Spatial distribution of diatom carbon biomass normalized to total autotrophic carbon biomass, AC_{Diat} /AC, in the euphotic layer across the frontal zone. Distributions of Chl *a* concentration and carbon biomass of autotrophic phytoplankton in the euphotic layer across the frontal zone calculated using Chl *a* fluorescence measurements are displayed in (**B**) and (**C**), respectively.

bands of *Syn* retrieved from the ALF spectral measurements (e.g. F_{PE1} and F_{PC}) showed similar trends.

The large increase in the F_{PE12}:SYN ratio with depth results in relatively low correlation between the two variables for the samples from various depths (R^2= 0.42; see linear regression in Fig. 5D). On the other hand, the subset of subsurface samples taken above the Chl *a* maxima, which shows low F_{PE12}:SYN variability (Fig. 7), yields a much better correlation between the F_{PE12} and SYN (black dots in Fig. 5D; R^2= 0.95). Consequently, we used the correlation for this near-surface data subset to convert the underway PE fluorescence measurements (4.5 m sampling depth) into high-resolution surface distributions of *Syn* carbon biomass (SYN_F) to analyze for structural changes in the autotrophic community across the frontal zone.

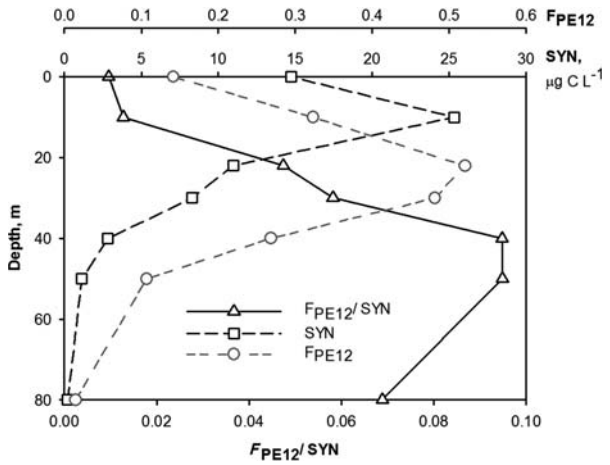

Fig. 7. An example of vertical distributions of *Syn*-specific phycoerythrin fluorescence (F_{PE12}), their carbon biomass (SYN) and the ratio of these variables (discrete samples from Station 8).

Underway fluorescence measurements

The surface distributions of Chl *a* concentration, autotroph and *Synechococcus* carbon biomass across the A-Front (Fig. 8) were calculated from the ALF fluorescence underway data using the regression relationships described in the previous section. As evident from Fig. 8, all of the variables exhibited considerable change across the frontal zone. In particular, the surface magnitudes of C_{Fchl} were 4-fold higher (0.7–0.8 µg C L^{-1}) in the northern area than the southern waters (~0.2 µg C L^{-1}). Similarly, the surface magnitudes of AC_F were ~3-fold higher north of the front compared with the lowest southern values observed around 32.68°N (35 versus 12 µg C L^{-1}, respectively). The north–south difference in surface CDOM fluorescence, F_{CDOM}, was smaller but still substantial (~2-fold; Fig. 8A).

The F_{PE1} fluorescence of the blue-water *Syn* (Fig. 8B) was also three to five times higher in the more productive northern area, where the strong subsurface F_{PE1} maximum was detected in discrete water samples (Fig. 4A). The surface maximum of F_{PE1} was less intense and spatially shifted relative to the subsurface F_{PE1} maximum (32.795°N versus 32.86°N, respectively). The F_{PE1} variability in surface waters adjacent to the A-Front showed similarity to the distribution of seasurface salinity (SSS). Indeed, F_{PE1} and SSS co-varied over most of the transect, had their local maxima in close proximity in northern and southern areas and showed very sharp changes at the front (32.762°N; Fig. 8B, insert). The seasurface temperature (SST) patterns were generally less complex, declining gradually from 16.9 to 15.4C between 32.67 and 32.762 °N and showing little variability in the northern area.

In the surface oligotrophic waters south of the A-Front, F_{PE2} fluorescence of green-water *Syn* was low, below the threshold for reliable detection (Fig. 8B). Following the trends for F_{PE1}, it also showed a sharp frontal peak at 32.764 °N, reached its maximum intensity around the SSS peak at 32.776 °N, and displayed little spatial variability north of that location. F_{PE3} fluorescence of cryptophytes was also undetectable between 32.67 and 32.74 °N, and increased gradually with declining SST and SSS in the frontal zone (see Fig. 8B). North of the A-Front, F_{PE3} fluorescence had a local maximum between 32.77 and 32.81 °N, declined somewhat around 32.825 °N, and increased gradually to the north.

The underway estimates of SYN_F biomass (red right axis in Fig. 8B) varied from 2.5–3.0 µg C L^{-1} in the southern portion of the transect to 10–14 µg C L^{-1} in the north, with a peak magnitude of ~16 µg C L^{-1}. Using the SYN_F and AC_F fluorescence estimates to assess structural changes in the surface autotrophic community, *Syn* comprised 40–45% of the total biomass of autotrophs over a considerable portion of the northern area between 32.78 and 32.84 °N (displayed with dark green in Fig. 8A). This relative contribution declined gradually to 25% toward the A-Front and to 30% in the most northern portion of the survey area. In the south, SYN/AC values varied around 20% between 32.67 and 32.74°N, and declined to 7% in the frontal zone, following the respective changes in SST and SSS.

DISCUSSION

Three distinct autotrophic communities were identified along the 25-km frontal transect from the ALF fluorescence measurements. The warm oligotrophic surface waters to the south of the front were characterized by relatively low levels of Chl *a*, total autotrophic and *Synechococcus* carbon biomass (C_{Fchl}, AC_F and SYN_F respectively). Green-water types of *Synechococcus* and cryptophytes were virtually absent south of the front; total SYN biomass did not exceed 20% of autotrophic carbon in the surface waters (Fig. 8). A distinct minimum of F_v/F_m in the subsurface Chl *a* maximum south of the front (Fig. 3) suggested nutrient limitation of phytoplankton growth. Consistent with the fluorescence characterization of the oligotrophic status of the southern area, FCM and HPLC pigment analyses showed that *Prochlorococcus* spp. comprised an important component of the autotrophic community there, up to 25% of euphotic zone carbon biomass, whereas these small phototrophic bacteria were largely absent from

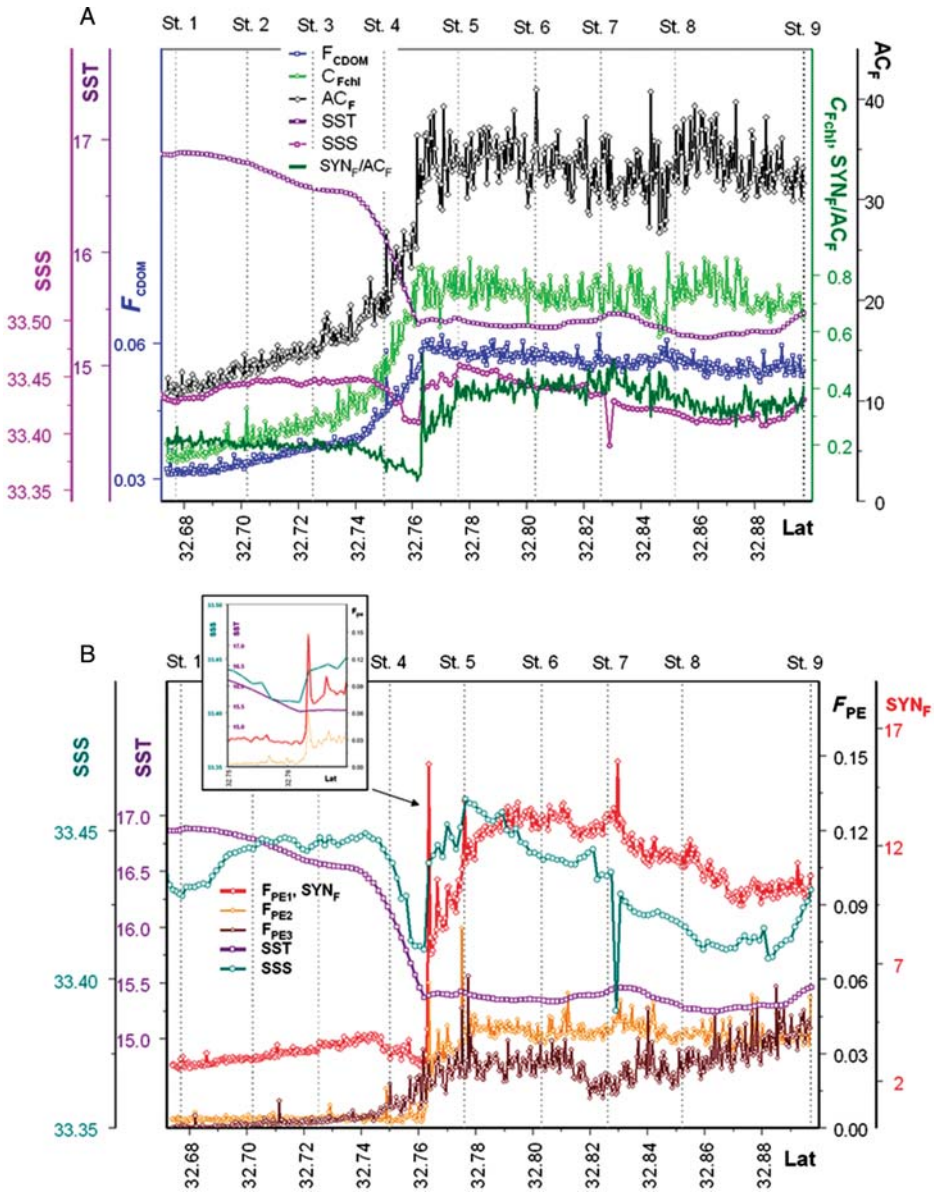

Fig. 8. Surface distributions across the A-Front retrieved from the ALF underway measurements. Dashed vertical lines display locations of stations 1–9 (Fig. 1) sampled after conducting the underway measurements. (**A**) CDOM fluorescence (F_{CDOM}), and fluorescence assessments of Chl *a* concentration (C_{Fchl}, μg L^{-1}), phytoplankton carbon biomass (AC_B μg C L^{-1}), and the relative *Syn* contribution to the total autotrophic carbon biomass (SYN_F/AC_B dark green). (**B**) PE fluorescence of blue-water and green-water types of *Syn* (F_{PE1} and F_{PE2}, respectively) and cryptophytes (F_{PE3}). *Syn* carbon biomass (SYN_B μg C L^{-1}; red vertical scale) was calculated from F_{PE1} data. The underway measurements of SSS and SST indicate location of the frontal feature between stations 4 and 5.

the frontal and northern stations (Taylor *et al.*, 2012). The nanoflagellate-dominated assemblage below 40 m in the southern region showed notably higher fluorescence per unit of phytoplankton carbon (Fig. 5C). This could be caused by physiological differences in the phytoplankton assemblage sampled in these waters that represented the low-salinity signature of the California Current. The elevated values of variable fluorescence found in these waters are consistent with such an interpretation. As suggested by Landry, Ohman *et al.*, (2012), southern waters with these isopycnal characteristics (24.7–24.8) could be a source of dissolved iron, thus resulting in higher phytoplankton photochemical efficiency in the frontal region.

Compared to the southern waters, surface waters on the cooler northern side of the A-Front had 3–4-fold higher concentrations of Chl *a* and phytoplankton carbon biomass (Figs 6 and 8). A strong subsurface maximum of PBP fluorescence at 20–30 m depth was found north of the front as well (Fig. 4). ALF spectral

analysis indicated that the blue-water *Syn* was very abundant in the core of this maximum, while green-water *Syn* and cryptophytes were less abundant, occupying spatially separated water patches on either side of the blue-water *Syn* core. The mechanisms driving the observed structural variability in the PBP-containing phytoplankton community remain unclear and need further investigation. Based on the FCM data of Taylor *et al*. (Taylor *et al*., 2012), *Syn* were indeed overwhelmingly dominant in the subsurface pigment maximum in the northern area, comprising over 80% of AC around the core of the F_{PE1} fluorescence maximum, and 30–45% of AC in the surface waters. The measurements of variable fluorescence (F_v/F_m) indicated a moderate, though not optimal, photophysiological status of phytoplankton community, consistent with the low concentrations of nitrate (0.2–0.3 μM) in mixed-layer waters.

The frontal feature (stations 4 and 5) was defined by a strong subsurface maximum of Chl *a* fluorescence at 20–40 m depth that yielded estimates of C_{Fchl} ~1.6 μg L^{-1} and AC_F ~85 μg C L^{-1} (Figs 3 and 6B and C). According to microscopic analyses (Taylor *et al*., 2012), large diatoms dominated the maximum, comprising ~90% of total autotroph carbon at their peak concentration (Fig. 6A). The reduction in biomass of blue-water *Syn* accompanied by the appearance of green-water *Syn* and cryptophytes were other distinct structural features of the front gradient observed while approaching it from the south (Fig. 8). As noted by Taylor *et al*. (Taylor *et al*., 2012), cell abundances and associated pigments (divinyl Chl *a*, zeaxanthin) of all phototrophic bacteria were markedly depressed at the A-Front stations. The frontal zone of enhanced biomass was also marked by the highest values of F_v/F_m (≥0.4) measured on the transect (Fig. 3B). The covariation of F_v/F_m with nitrate concentration in this layer (Fig. 3B), along with the structural changes in phytoplankton community, suggest that it had been generated by *in situ* processes rather than advection. The elevated phytoplankton biomass and photophysiological functionality in the frontal zone was attributed by Li *et al*. (Li *et al*., 2012) to the nutrient enrichment by the diapycnal nitrate fluxes. This interpretation is consistent with previous field studies showing a link between photophysiological status of phytoplankton and nutrient supply (e.g. Falkowski *et al*., 1991; Falkowski and Kolber, 1995). On the other hand, as shown by Suggett *et al*. (Suggett *et al*., 2009), the magnitudes of photophysiological variability driven by structural changes in a phytoplankton community often exceed those induced by nutrient conditions. Thus, both nutrient enrichment and structural changes in the autotrophic population need to be accounted for to explain the elevated values of F_v/F_m detected at the front.

The high-resolution underway ALF measurements revealed fine-scale surface structures across the frontal zone, notably the abrupt peak in *Syn* biomass at the location of the strong frontal gradient in SSS (Fig. 8B insert), that discrete sampling would not have shown. Sharply elevated *Syn* concentrations, indicated by F_{PE1} and F_{PE2}, occurred right at the break point, where salinity increased sharply from a substantial surface minimum. This suggests a narrow zone (~100 m width), where some lower-salinity water (a signature of the California Current proper) was brought into the frontal surface mixed layer from 40 to 70 m depth on the south side. Such an intrusion is implied in the salinity section (Fig. 2A), but cannot be seen clearly due to the coarse resolution of the transect station sampling. Nonetheless, the profile resolution is sufficient to note upwardly sloping isopycnal and nutrient surfaces in this vicinity. Thus, the mixed-layer transition in cyanobacterial biomass and composition, as well as the subsurface maxima in Chl *a* concentration, phytoplankton biomass and diatoms at the front (Fig. 6) may all be sustained by an intrusion of nutrient-rich, lower-salinity water that comes from the southern side of the frontal boundary (Li *et al*., 2012). In contrast to the sharp frontal gradient in *Syn* biomass, both Chl *a* concentration and autotroph biomass exhibited rather gradual, though substantial change across the frontal zone (Fig. 8A), consistent with the satellite observations (Li *et al*., 2012). Similar patterns were detected by the ALF underway measurements when crossing frontal features at other locations in the California Current System (data not shown). Understanding the origin of different responses of phototrophic cyanobacteria and eukaryotic phytoplankton in frontal areas may provide new insights regarding physico-chemical and biological interactions in the ocean.

Several methodological findings have resulted from the opportunity to assess ALF data in conjunction with contemporaneous analyses of phytoplankton pigments, biomass and composition by HPLC, FCM and microscopy. Despite significant variability in phytoplankton composition (Taylor *et al*., 2012) and photophysiology (Fig. 3B) across the frontal zone, we found a linear regression relationship between Chl *a* fluorescence and total autotrophic carbon biomass (AC) among the different plankton habitats and depths examined. In this study, the ALF *in vivo* Chl *a* fluorescence measurements were more highly correlated with AC (Fig. 5C) than the HPLC assessments of extracted Chl *a* (R^2= 0.79 versus 0.49, respectively). Our field observations are consistent with the recent laboratory measurements and growing

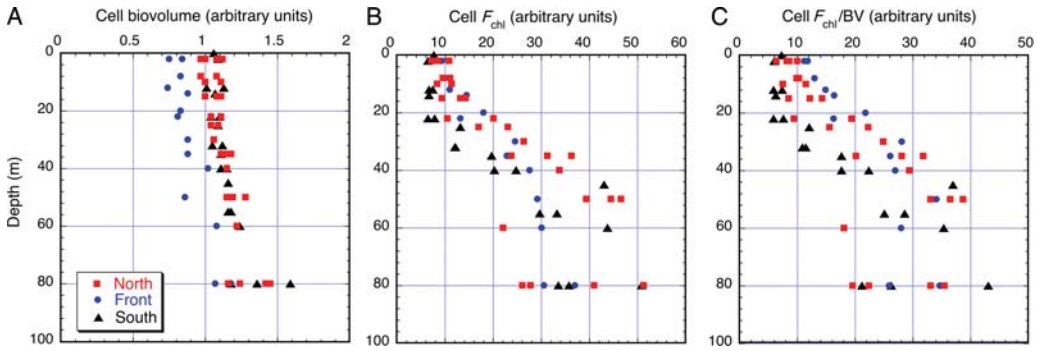

Fig. 9. Cell size and pigment content variations of *Synechococcus* spp. with depth based on flow cytometric analyses of samples collected at stations north, south and at the front (Fig. 1). (**A**) Relative estimates of cell BV based on bead-normalized measurements of Forward Angle Light Scatter (BV = FALS$^{0.55}$). (**B**) Relative estimates of cell pigment content based on bead-normalized measurements of cell Chl *a* fluorescence (F_{chl}). (**C**) Estimates of cell pigment to BV ratio. All data are arbitrary bead-normalized units.

understanding that *in vivo* Chl *a* fluorescence may provide more accurate AC assessments than concentration of extracted Chl *a* (e.g. Kruskopf and Flynn, 2006; Proctor and Roesler, 2010).

The strong, though non-linear, relationship between the F_{chl} and C_{chl} measurements (e.g. $R^2 = 0.95$, Fig. 5A) indicates that *in vivo* spectral measurements of Chl *a* fluorescence from dark-adapted phytoplankton can be used for accurate assessments of Chl *a* concentration. This is consistent with our earlier ALF measurements in estuarine and coastal waters and analysis of spectral and photo-physiological variability in fluorescence signatures (Chekalyuk and Hafez, 2008, 2011). Interestingly, samples from the Chl *a* maximum at the front, which were dominated by large diatoms, showed a ~50% higher F_{chl}:C_{chl} ratio (Fig. 5B). The interpretation of this frontal feature is not straightforward. Generally, the F_{chl}:C_{chl} values can vary over a wide range, depending on phytoplankton taxonomic composition, cell size and physiological state (e.g. Falkowski and Kiefer, 1985; MacIntyre *et al.*, 2010; Proctor and Roesler, 2010; Lawrenz and Richardson, 2011). Physiological variability has been shown to markedly increase the F_{chl}:C_{chl} ratio under nutrient-starved conditions (MacIntyre *et al.*, 2010), which was not the case in the frontal Chl *a* maximum as evident from the nitrate and F_v/F_m patterns (see Fig. 3B and the relevant discussion). The diatoms that overwhelmingly dominated the frontal Chl *a* maximum had larger cell size compared to dominant nanoplankton and picoplankton dominated outside the frontal Chl *a* maximum (Taylor *et al.*, 2012). Therefore, the packaging effect (Morel and Bricaud, 1981; Kirk, 1994), which leads to the F_{chl}:C_{chl} ratio decreasing for larger phytoplankton cells (e.g. Proctor and Roesler, 2010; Lawrenz and Richardson, 2011), should result in lower F_{chl}:C_{chl} values in the frontal Chl *a* maximum. We believe that the different taxonomic composition of phytoplankton assemblages inside and outside the frontal Chl *a* maximum was the main factor that resulted in the distinct differences in F_{chl}:C_{chl} ratios between these areas, overriding the packaging effect. In particular, *Syn* were practically absent in the diatom-dominated frontal pigment maximum (Fig. 6A), but they comprised a significant portion of phytoplankton biomass outside the frontal feature [20–40% in the surface waters (Fig. 8A), and up to 85% (data of Taylor *et al.*, 2012) in the spatially extended NF subsurface maximum (Fig. 4)]. These cyanobacteria have significantly lower proportions of Chl *a* associated with photosystem II (PSII) than eukaryotic phytoplankton (Johnsen and Sakshaug, 2007). Since most Chl *a* fluorescence originates from PSII (Krause and Weis, 1991), this typically results in much lower F_{chl}:C_{chl} ratio for cyanobacteria versus eukaryotic phytoplankton (e.g. Lawrenz and Richardson, 2011). Thus, the distinctly different F_{chl}:C_{chl} values that we found inside and outside the frontal Chl *a* maximum are potentially explained by variations in the relative abundances of *Syn* in the euphotic layer across the frontal zone.

While a strong linear relationship between *Syn*-specific PE fluorescence and estimates of *Syn* carbon biomass was found within the subsurface mixed layer, a substantial increase in the F_{PE12}:SYN ratio with depth was consistently observed below the mixed layer. Complementary flow-cytometric estimates of bead-normalized cell size (from forward angle light scatter, FALS) and bead-normalized pigment content (cellular Chl *a* fluorescence, F_{chl}) (Fig. 9) may help in assessing the factors that affected the variable relationship between SYN biomass and fluorescence with depth. FALS as an index of relative cell BV (Binder *et al.*, 1996; Landry *et al.*, 2003) showed a relatively small, ~50%, increase with depth (Fig. 9A). In addition, the *Syn* cells size was found to be smaller at the front

compared to adjacent northern and southern waters. However, much stronger alterations were observed in cell pigment content (Fig. 9B), which increased by a factor of 3–5 from the surface to the deep euphotic zone and dominated the resulting variability of the cellular F_{chl}:BV ratio (Fig. 9C). None of these variable factors was reflected in our simplified SYN estimates (Taylor *et al.*, 2012). The lowest near-surface variability evident in Fig. 9 may thus explain the tight statistical relationship between SYN and *Syn*-specific PE fluorescence in the upper mixed layer (Fig. 5D).

CONCLUSIONS

In the present study, we employed a new analytical technique, ALF, to investigate the spatial variability of phytoplankton characteristics across a frontal zone in the southern California Current ecosystem. We used the ALF *in vivo* fluorescence measurements to assess the spatial patterns of fluorescence associated with Chl *a* concentration, phytoplankton carbon biomass, photophysiology, group-specific PBP pigments and CDOM along the A-Front sampling transect. We detected sharp transitions in physical and biological parameters that separate warmer oligotrophic waters to the south from cooler mesotrophic waters in the north, with a zone of enhanced biomass and photophysiological potential at the frontal interface. While large diatoms were overwhelmingly dominant in this strong subsurface biomass maximum at the front, the blue-water type of *Synechococcus*, accompanied by PBP-containing cryptophytes, dominated phytoplankton biomass in a shallow pigment maximum north of the front. In contrast, only blue-water *Synechococcus* at 4-fold lower concentration were detected among PBP-containing groups in the oligotrophic water south of the front; the Chl *a* maximum here coincided spatially with low nutrient concentration and depressed photophysiological state of the phytoplankton. The abrupt frontal peak in *Synechococcus* biomass was detected by high-frequency ALF underway surface measurements in a narrow (~100 m width) zone of lower-salinity California Current water brought into the surface from depth. The results of this study, whether interpreted in terms of the primary fluorescence measurements or the calibrated data products, revealed strong biological responses of phytoplankton communities to the frontal changes in physical and chemical properties.

In this study, ALF measurements compared well with contemporaneous analyses of phytoplankton concentration, biomass and composition by HPLC (pigments), FCM and microscopy despite considerable variability in phytoplankton composition (Taylor *et al.*, 2012) and photophysiology across the frontal zone. The advantage of the ALF technique is that it provides real-time *in vivo* spectral analysis for characterizing variability of the phytoplankton community. Such measurements can be conducted in variety of instrument configurations and settings, including the benchtop measurements reported here, *in situ* fluorometers and remote LIDAR fluorosensors (e.g. Cowles *et al.*, 1993; Chekalyuk *et al.*, 1995; Wright *et al.*, 2001). Recent advances in laser technology and spectroscopy allow for the development of new compact and affordable field spectrofluorometers for oceanographic research and environmental monitoring.

ACKNOWLEDGEMENTS

We thank the captain and crew of the R/V *Melville* and all participants in the CCE-LTER process cruises. Our special thanks to Mark Ohman, Greg Mitchell, Haili Wang, Brian Seegers and Megan Roadman for their support of the ALF measurements in the California Current System, and Konstantin Semyanov for his technical assistance and participation in the ALF measurements on the cruise. We thank Michael Roberto for his notes and assistance editing the manuscript and three anonymous reviewers for their insightful comments to improve the manuscript.

FUNDING

This research was supported by grants to A.C. from NSF (Ocean Technology and Interdisciplinary Coordination program; OCE-07-24561) and NASA (Ocean Biology and Biogeochemistry Program; NNX07AN44G), and by NSF funding for the CCE LTER Program (OCE 04-17616 and 10-26607).

REFERENCES

Ashjian, C. J., Davis, C. S., Gallager, S. M. *et al.* (2005) Characterization of the zooplankton community, size composition, and distribution in relation to hydrography in the Japan/East Sea. *Deep-Sea Res. II*, **52**, 1363–1392.

Baird, M. E., Timko, P. G., Middleton, J. H. *et al.* (2008) Biological properties across the Tasman Front off southeast Australia. *Deep Sea Res. I*, **55**, 1438–1455.

Belkin, I. M., Cornillon, P. C. and Sherman, K. (2009) Fronts in large marine ecosystems. *Prog. Oceanogr.*, **81**, 223–236.

Binder, B. J., Chisholm, S. W., Olson, R. J. *et al.* (1996) Dynamics of picophytoplankton, ultaphytoplankton and bacteria in the central equatorial Pacific. *Deep-Sea Res. II*, **43**, 907–931.

Bost, C. A., Cotte, C., Bailleul, F. *et al.* (2009) The importance of oceanographic fronts to marine birds and mammals of the southern oceans. *J. Mar. Syst.*, **78**, 363–376.

Boucher, J., Ibanez, F. and Prieur, L. (1987) Daily and seasonal variations in the spatial distribution of zooplankton populations in relation to the physical structure in the Ligurian front. *J. Mar. Res.*, **45**, 133–173.

Bricaud, A., Babin, M., Morel, A. *et al.* (1995) Variability in the chlorophyll-specific absorption coefficients of natural phytoplankton: analysis and parameterization. *J. Geophys. Res.*, **100**, 13321–13332.

Brown, S. L., Landry, M. R., Selph, K. E. *et al.* (2008) Diatoms in the desert: phytoplankton community response to a mesoscale eddy in the subtropical North Pacific. *Deep-Sea Res. II*, **55**, 1321–1333.

Chekalyuk, A. M., Demidov, A. A. and Fadeev, V. V. (1995) Lidar monitoring of phytoplankton and organic matter in the inner seas of Europe. *EARSeL Adv. Remote Sensing*, **3**, 131–139.

Chekalyuk, A. M. and Hafez, M. (2008) Advanced laser fluorometry of natural aquatic environments. *Limnol. Oceanogr. Meth.*, **6**, 591–609.

Chekalyuk, A. M. and Hafez, M. (2011) Photo-physiological variability in phytoplankton chlorophyll fluorescence and assessment of chlorophyll concentration. *Opt. Express*, **19**, 22643–22658.

Claustre, H., Kerherve, P., Marty, J. C. *et al.* (1994) Phytoplankton dynamics associated with a geostrophic front: ecological and biogeochemical implications. *J. Mar. Res.*, **52**, 711–742.

Corredor, J., Morell, J., Lopez, J. *et al.* (1987) Daily and seasonal variations in the spatial distribution of zooplankton populations in relation to the physical structure in the Ligurian front. *Geophys. Res. Lett.*, **30**, 2057.

Cowles, T. J., Desiderio, R. A. and Neuer, S. (1993) In situ characterization of phytoplankton from vertical profiles of fluorescence emission spectra. *Mar. Biol.*, **115**, 217–222.

Davis, R. E., Ohman, M. D., Rudnick, D. L. *et al.* (2008) Glider surveillance of physics and biology in the southern California Current System. *Limnol. Oceanogr.*, **53**, 2151–2168.

Falkowski, P. G. and Kiefer, D. A. (1985) Chlorophyll a fluorescence in phytoplankton: relationship to photosynthesis and biomass. *J. Plankton Res.*, **7**, 715–731.

Falkowski, P. G. and Kolber, Z. (1995) Variations in chlorophyll fluorescence yields in phytoplankton in the world oceans. *Aust. J. Plant Physiol.*, **22**, 341–355.

Falkowski, P. G., Ziemann, D., Kolber, Z. *et al.* (1991) Role of eddy pumping in enhancing primary production in the ocean. *Nature*, **352**, 55–58.

Fernandez, E. and Pingree, R. D. (1996) Coupling between physical and biological fields in the North Atlantic subtropical front southeast of the Azores. *Deep-Sea Res. I.*, **43**, 1369–1393.

Frajka-Williams, E., Rhines, P. B. and Eriksen, C. C. (2009) Physical controls and mesoscale variability in the Labrador Sea spring phytoplankton bloom observed by Seaglider. *Deep-Sea Res. I*, **56**, 2144–2161.

Franks, P. J. S. (1992a) Sink or swim: accumulation of biomass at fronts. *Mar. Ecol. Prog. Ser.*, **82**, 1–12.

Franks, P. J. S. (1992b) Phytoplankton blooms at fronts: patterns, scales and physical forcing mechanisms. *Rev. Aquat. Sci.*, **6**, 121–137.

Garrison, D. L., Gowing, M. M., Hughes, M. P. *et al.* (2000) Microbial food web structure in the Arabian Sea: a US JGOFS study. *Deep-Sea Res. II*, **47**, 1387–1422.

Goericke, R. (2002) Top-down control of phytoplankton biomass and community structure in the monsoonal Arabian Sea. *Limnol. Oceanogr.*, **47**, 1307–1323.

Haury, L. R., Venrick, E. L., Fey, C. L. *et al.* (1993) The Ensenada Front: July 1985. *CalCOFI Rep.*, **34**, 69–88.

Hitchcock, G. L., Rossby, T., Lillibridge III, J. L. *et al.* (1994) Signatures of stirring and mixing near the Gulf-Stream front. *J. Mar. Res.*, **52**, 797–836.

Hodges, B. A. and Fratantoni, D. M. (2009) A thin layer of phytoplankton observed in the Philippine Sea with a synthetic moored array of autonomous gliders. *J. Geophys. Res.*, **114**, C10020 (1-15).

Hoge, F. E. and Swift, R. N. (1981) Airborne simultaneous spectroscopic detection of laser-induced water Raman backscatter and fluorescence from chlorophyll a and other naturally occurring pigments. *Appl. Optics*, **20**, 3197–3205.

Hoge, F. E. and Swift, R. N. (1983) Airborne dual laser excitation and mapping of phytoplankton photo-pigments in a Gulf-Stream Warm Core Ring. *Appl. Optics*, **22**, 2272–2281.

Holeton, C. L., Nedelec, F., Sanders, R. *et al.* (2005) Physiological state of phytoplankton communities in the Southwest Atlantic sector of the Southern Ocean, as measured by fast repetition rate fluorometry. *Polar Biol.*, **29**, 44–52.

Hood, R. R., Neuer, S. and Cowles, T. J. (1992) Autotrophic production, biomass and species composition at 2 stations across an upwelling front. *Mar. Ecol. Prog. Ser.*, **83**, 221–232.

Jacquet, S., Prieur, L., Avois-Jacquet, C. *et al.* (2002) Short-timescale variability of picophytoplankton abundance and cellular parameters in surface waters of the Alboran Sea (western Mediterranean). *J. Plankton Res.*, **24**, 635–651.

James, C., Tomczak, M., Helmond, I. *et al.* (2002) Summer and winter surveys of the Subtropical Front of the southeastern Indian Ocean 1997–1998. *J. Mar. Syst.*, **37**, 129–149.

Johnsen, G. and Sakshaug, E. (2007) Biooptical characteristics of Psii and Psi in 33 species (13 pigment groups) of marine phytoplankton, and the relevance for pulse-amplitude-modulated and fast-repetition-rate fluorometry. *J. Phycol.*, **43**, 1236–1251.

Johnston, T. M. S., Cheriton, O. M., Pennington, J. T. *et al.* (2009) Thin phytoplankton layer formation at eddies, filaments, and fronts in a coastal upwelling zone. *Deep-Sea Res. II*, **56**, 246–259.

Kahru, M., Di Lorenzo, E., Manzano-Sarabia, M. *et al.* (2012) Spatial and temporal statistics of sea surface temperature and chlorophyll fronts in the California Current. *J. Plankton Res.*, **34**, 749–760.

Kiefer, D. A. (1973) Fluorescence properties of natural phytoplankton populations. *Mar. Biol.*, **22**, 263–269.

Kirk, J. T. O. (1994) *Light and Photosynthesis in Aquatic Ecosystems*, Cambridge University Press.

Klyshko, D. N. and Fadeev, V. V. (1978) Remote determination of concentration of impurities in water by the laser spectroscopy method with calibration by Raman scattering. *Sov. Phys. Dokl.*, **23**, 55–59.

Krause, G. H. and Weis, E. (1991) Chlorophyll fluorescence and photosynthesis - the basics. *Annu. Rev. Plant Phys.*, **42**, 313–349.

Kruskopf, M. and Flynn, K. J. (2006) Chlorophyll content and fluorescence responses cannot be used to gauge reliably phytoplankton biomass, nutrient status or growth rate. *New Phytol.*, **169**, 525–536.

Landry, M. R., Brown, S. L., Neveux, J. *et al.* (2003) Phytoplankton growth and microzooplankton grazing in high-nutrient, low-chlorophyll waters of the equatorial Pacific: community and taxon-specific rate assessments from pigment and flow cytometric analyses. *J. Geophys. Res.*, **108**(C12), 8142, doi:10.1029/2000JC000744.

Landry, M. R., Brown, S. L., Rii, Y. M. *et al.* (2008) Depth-stratified phytoplankton dynamics in Cyclone Opal, a subtropical mesoscale eddy. *Deep-Sea Res. II*, **55**, 1348–1359.

Landry, M. R., Brown, S. L., Selph, K. E. *et al.* (2001) Initiation of the spring phytoplankton increase in the Antarctic Polar Front Zone at 170°W. *J. Geophys. Res.*, **106**, 13903–13915.

Landry, M.R., Ohman, M.D., Goericke, R. *et al.* (2012) Pelagic community responses to a deep-water frontal system in the California Current Ecosystem: overview of the A-Front Study. *J. Plankton Res*, **34**, 739–748.

Landry, M. R., Selph, K. E., Brown, S. L. *et al.* (2002) Seasonal dynamics of phytoplankton in the Antarctic Polar Front region at 170°W. *Deep-Sea Res. II*, **49**, 1843–1865.

Lawrenz, E. and Richardson, T. L. (2011) How does the species used for calibration affect chlorophyll a measurements by in situ fluorometry?. *Estuarine Coast.*, **34**, 872–883.

Li, Q. P., Franks, P. J. S., Ohman, M. D. *et al.* (2012) Enhanced nitrate fluxes and biological processes at a frontal zone in the Southern California Current System. *J. Plankton Res*, **34**, 790–801.

Llido, J., Machu, E., Sudre, J. *et al.* (2004) Variability of the biological front south of Africa from SeaWiFS and a coupled physical-biological model. *J. Mar. Res.*, **62**, 595–609.

MacIntyre, H. L., Lawrenz, E. and Richardson, T.L. (2010) Taxonomic Discrimination of Phytoplankton by Spectral Fluorescence. In Suggett, D. J., Prasil, O. and Borowitzka, M. A. (eds), *Chlorophyll a Fluorescence in Aquatic Sciences: Methods and Applications: Methods and Applications*, Springer, Dordrecht, pp. 129–169.

Marra, J. (1997) Analysis of diel variability in chlorophyll fluorescence. *J. Mar. Res.*, **55**, 767–784.

Menden-Deuer, S. and Lessard, E. J. (2000) Carbon to volume relationships for dinoflagellates, diatoms, and other protist plankton. *Limnol. Oceanogr.*, **45**, 569–679.

Moore, C. M., Suggett, D., Holligan, P. M. *et al.* (2003) Physical controls on phytoplankton physiology and production at a shelf sea front: a fast repetition-rate fluorometer based field study. *Mar. Ecol. Prog Ser.*, **259**, 29–45.

Morel, A. and Bricaud, A. (1981) Thoeretical results concerning light absorption in a discrete medium and application to specific absorption of phytoplankton. *Deep-Sea Res.*, **28**, 1375–1393.

Niiler, P. P., Poulain, P. M. and Haury, L. R. (1989) Synoptic three-dimensional circulation in an onshore flowing filament of the California Current. *Deep-Sea Res.*, **36**, 385–405.

Ohman, M.D., Powell, J., Picheral, M. *et al.* (2012) Mesozooplankton and particulate matter responses to a deep-water frontal system in the southern California Current System. *J. Plankton Res*, **34**, 815–827.

Olson, R. J., Sosik, H. M., Chekalyuk, A. M. *et al.* (2000) Effects of iron enrichment on phytoplankton in the Southern Ocean during late summer: active fluorescence and flow cytometric analyses. *Deep-Sea Res. II*, **47**, 3181–3200.

Proctor, C. W. and Roesler, C. S. (2010) New insights on obtaining phytoplankton concentration and composition from in situ multispectral Chlorophyll fluorescence. *Limnol. Oceanogr. Meth.*, **8**, 695–708.

Read, J. F., Pollard, R. T. and Bathmann, U. (2002) Physical and biological patchiness of an upper ocean transect from South Africa to the ice edge near the Greenwich Meridian. *Deep-Sea Res. II*, **49**, 3713–3733.

Selph, K. E., Landry, M. R., Taylor, A. G. *et al.* (2011) Spatially-resolved taxon-specific phytoplankton production and grazing dynamics in relation to iron distributions in the Equatorial Pacific between 110 and 140°W. *Deep-Sea Res. II*, **58**, 358–377.

Sherr, E. B. and Sherr, B. F. (1993) Preservation and storage of samples for enumeration of heterotrophic protists. In Kemp, P. K. (ed.), *Handbook of Methods in Aquatic Microbial Ecology*. CRC Press, Boca Raton, FL, pp. 207–212.

Stramska, M. and Dickey, T. D. (1992) Variability of bio-optical properties of the upper ocean associated with diel cycles in phytoplankton population. *J. Geophys. Res. Oceans*, **97**, 17873–17887.

Strutton, P. G., Mitchell, J. G., Parslow, J. S. *et al.* (1997) Phytoplankton patchiness: quantifying the biological contribution using fast repetition rate fluorometry. *J. Plankton Res.*, **19**, 1265–1274.

Suggett, D. J., Moore, C. M., Hickman, A. E. *et al.* (2009) Interpretation of fast repetition rate (FRR) fluorescence: signatures of phytoplankton community structure versus physiological state. *Mar. Ecol. Prog Ser.*, **376**, 1–19.

Taylor, A. G., Goericke, R., Landry, M. R. *et al.* (2012) Sharp gradients in phytoplankton community structure across a frontal zone in the California Current Ecosystem. *J. Plankton Res*, **34**, 778–789.

Taylor, A. G., Landry, M. R., Selph, K. E. *et al.* (2011) Biomass, size structure and depth distributions of the microbial community in the eastern equatorial Pacific. *Deep-Sea Res. II*, **58**, 342–357.

Trees, C. C., Aiken, J., Hirche, H. *et al.* (1992) Biooptical variability across the Arctic Front. *Polar Biol.*, **12**, 455–461.

Vaillancourt, R. D., Marra, J., Seki, M. P. *et al.* (2003) Impact of a cyclonic eddy on phytoplankton community structure and photosynthetic competency in the subtropical North Pacific Ocean. *Deep-Sea Res. I*, **50**, 829–847.

Venrick, E. L. (2000) Summer in the Ensenada front: the distribution of phytoplankton species, July 1985 and September 1988. *J. Plankton Res.*, **22**, 813–841.

Vernet, M., Mitchell, B. G. and Holm-Hansen, O. (1990) Adaptation of *Synechococcus* in situ determined by variability in intracellular phycoerythrin-543 at a coastal station off the Southern California coast, USA. *Mar. Ecol. Prog Ser.*, **5**, 9–16.

Wright, C. W., Hoge, F. E., Swift, R. N. *et al.* (2001) Next generation NASA airborne oceanographic lidar system. *Appl. Opt.*, **40**, 336–342.

Yu, X. R., Dickey, T., Bellingham, J. *et al.* (2002) The application of autonomous underwater vehicles for interdisciplinary measurements in Massachusetts and Cape Cod Bays. *Cont. Shelf Res.*, **22**, 2225–2245.

Zhai, L., Platt, T., Tang, C. *et al.* (2011) Phytoplankton phenology on the Scotian Shelf. *ICES J. Mar. Sci.*, **68**, 781–791.